Synthesis of Bulk Amorphous Alloy from Fe-Base Powders by Explosive Consolidation

Jianbin Li, Ming Lu *, Yongbao Ai, Cong Tao and Yun Xiong

Field Engineering College, Army Engineering University of PLA, Nanjing 210007, China;
lijianbin0416@163.com (J.L.); aybjackai@126.com (Y.A.); sdffvgs@foxmail.com (C.T.); xy820507@163.com (Y.X.)
* Correspondence: luming569@sohu.com; Tel.: +86-180-1390-9679

Abstract: A $Fe_{61}Cr_2Nb_3Si_{12}B_{22}$ amorphous alloy rod sample of 8.8 mm diameter has been successfully prepared through explosive consolidation. The structure and thermal stability of the as-synthesized sample have been analyzed through X-ray diffraction (XRD) and differential scanning calorimeter (DSC) analysis. The results demonstrate that the sample still retains an amorphous structure, and the glass transition temperature (Tg), the crystallization onset temperature (Tx), the supercooled liquid zone (ΔTx) (Tx − Tg) and the reduced glass transition temperatures (Trg) (Tg/Tm) are 784 K, 812 K, 28 K, and 0.556, respectively. Its microstructure has been investigated by optical microscopy (OM) and scanning electron microscopy (SEM). The average microhardness of the alumina compact is about 1069 HV.

Keywords: Fe-based amorphous; explosive consolidation; bulk amorphous alloy

1. Introduction

Fe-based amorphous alloys, which are different from those of crystalline alloys for lack of long-range atomic order [1,2], have attracted increasing attention in recent years due to the high mechanical strength, strong corrosion resistance and good soft magnetic properties [3–6]. On the other hand, Fe-based alloys have a lower amorphous-forming ability and require a very fast cooling rate during cooling [7,8]. Usually, the cooling rate is required to be as high as 10^5–10^6 K s^{-1} [9]. Most Fe-based amorphous alloy samples are filaments or ribbons of 15 μm in maximum thickness [7]. At present, although amorphous ribbons have been widely utilized in transformer cores or noise suppression sheets, it is difficult to obtain large-sized devices due to the preparation condition constraints of amorphous alloys [10,11]. For this reason, Fe-based amorphous alloys are significantly limited in practical applications. Therefore, the preparation of a large-sized Fe-based bulk amorphous alloy has proven to be a quite significant research topic.

At present, the preparations of large-sized Fe-based bulk amorphous alloys are under study and a certain amount of progress has been made. Inoue et al. succeeded in preparing a $Fe_{60}Co_8Zr_{10}Mo_5W_2B_{15}$ amorphous alloy rod of 6 mm diameter through the copper mold casting method [12]. Lu et al. prepared a $Fe_{61}Y_2Zr_8Co_6Al_1Mo_7B_{15}$ amorphous alloy rod of 5 mm diameter through copper mold casting technology [13]. Poon et al. utilized a copper mold to cast a Fe-Mn-Cr-Mo-(Y, Ln)-C-B (Ln = Lanthanides) amorphous alloy rod of 6–7 mm diameter [14]. In addition to copper mold casting that used the rapid cooling and solidification of alloy, there are other methods for the preparation of Fe-based amorphous alloys. Li et al. prepared $Fe_{66}Co_{15}Mo_1P_{7.5}C_{5.5}B_2Si_3$ amorphous alloy rods of 2 mm diameter, utilizing Co to replace a portion of Fe and to purify the impurities of the melt [15]. From the viewpoint of stability improvement of ultra-cold liquids and the ability to form metallic glasses, Yang et al. enhanced the amorphous formation ability of Fe-based amorphous alloys through the addition of Cu [7]. Zhang et al. prepared a $(Fe, Co, Ni)_{75}P_{10}C_{10}B_5$ amorphous alloy rod of 1 mm maximum diameter through the

addition of microelements [16]. Paul et al. prepared a $Fe_{48}Cr_{15}Mo_{14}Y_2C_{15}B_6$ bulk amorphous alloy through spark plasma sintering technology [17]. For the aforementioned amorphous alloy preparation methods, the common point was to improve the amorphous formation ability of the alloy through increasing the cooling rate, or through the addition of nonmetallic elements such as B, C, Si and P, along with other metal elements such as Co, Ni and Cu, and amorphous alloys were prepared by the direct cooling of the liquid alloys. Above these preparation methods, because the principle of the preparation methods used rapid cooling and solidification, as a result, atoms of alloys cannot be ordered and crystallized, and the amorphous alloy size is relatively limited.

The explosive consolidation method is to load the instantaneous detonation energy to metal or non-metal powders, so that the powders are sintered between the powder particles to form a dense bulk [18]. The transient loading, promoting the relative movement of the particles, is responsible for a rapid energy deposition in the particle surface due to friction. Such rapid energy deposition is much faster than the energy diffusion throughout the particle body, leading to a temperature increase at the particle surface and, eventually, to melting. The time required for the powders at normal temperature to reach the melting point temperature is only microseconds. Therefore, the temperature increase of the powders is limited to the surface, and the thickness of the melted layer is approximately 0.5 μm, which is still relatively thin to the diameter of the powder particles. The interior of the powder particles maintains a low temperature, which will induce a cooling quenching effect on the sintered interface formed among the powder particles [19–21]. Compared with conventional preparation methods of amorphous alloys, this method can not only prevent the crystallization of powder particles caused by the slow cooling rate, ensuring the excellent characteristics of the metastable amorphous alloy, but can also consolidate different compositions of powders without considering the interactions between powder particles [22]. Owing to these characteristics, explosive consolidation has been researched. Wang utilized explosive consolidation to prepare a dense, high-volume Al_2O_3 rod with nanostructures [23]. Farinha et al. successfully synthesized two different sizes of stainless steel powders and produced crack-free blocks through explosive consolidation [24]. In this paper, based on the high strength of Fe-based amorphous alloys and the wide application prospect in functional materials, the investigation of explosive consolidation of amorphous powders is carried out to explore the explosive consolidation process of a large-sized Fe-based amorphous alloy.

2. Materials and Methods

Fe-based amorphous alloy powders supplied by Advanced Technology and Materials Co., Ltd. (Beijing, China) were prepared by mechanical crushing of amorphous ribbons. The mean size of powders observed by scanning electron microscopy (SEM; Hitachi S-4800, Tokyo, Japan) is 50 μm, as shown in Figure 1a. The chemical compositions of powders analyzed by Energy Dispersive Spectroscopy (EDS) are $Fe_{61}Cr_2Nb_3Si_{12}B_{22}$ (at. %), as shown in Figure 1b.

The diagram of an experimental device for explosive consolidation is shown in Figure 2. During the experiments, the Fe-based amorphous alloy powders (f) were packed in an end-sealed copper tube (e) of 9 mm inner diameter, 0.5 mm wall thickness and 120 mm length. The upper end of the copper tube was plug-sealed with a plug (d) of 15 mm length. Hydraulic compaction was also used to apply a certain pressure on the plug, in order to increase the initial density of the powders to 60% of theoretical density in the copper tube. An outer cylinder (b) of 80 mm diameter was placed on the steel baseplate (g). The copper tube with the powder was placed in the center of outer cylinder containing the emulsion explosive. The density of the emulsion explosive is about 0.9 g·cm^{-3} and the detonation velocity is about 3600 m·s^{-1}. Taking into account the influence of the unstabilized detonation section of the explosive on the quality of the powder in the copper tube, a 50-mm thick emulsion explosive was left between the detonator (a) and the upper end of the copper tube. The detonator was detonated and the detonation of the emulsion explosive caused a cylindrical compaction shock wave from the top to the bottom on the copper tube. The Fe-based amorphous powders filled in the copper tube were compressed instantaneously to form a dense rod alloy.
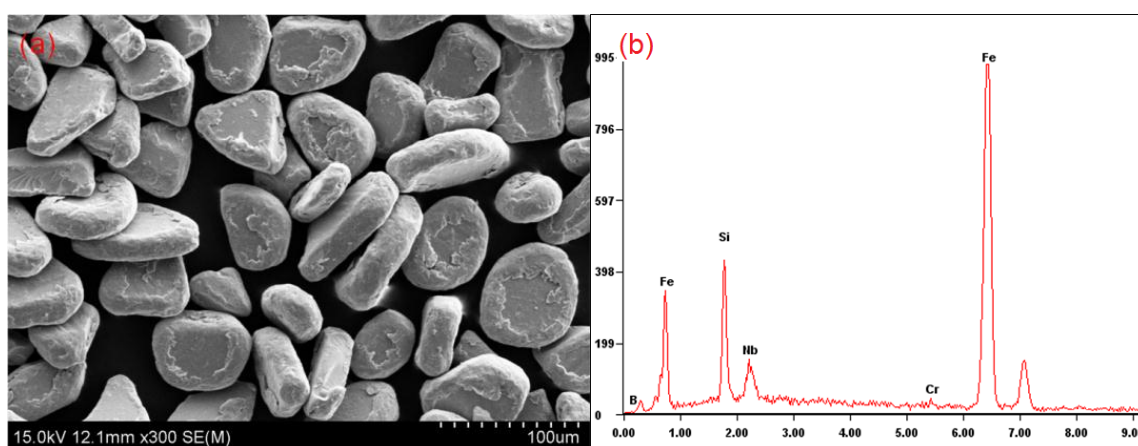
Figure 1. (**a**) SEM micrograph of the original powders, (**b**) peaks of elements.

(**a**)　　　　　　　　　　　　　　　(**b**)
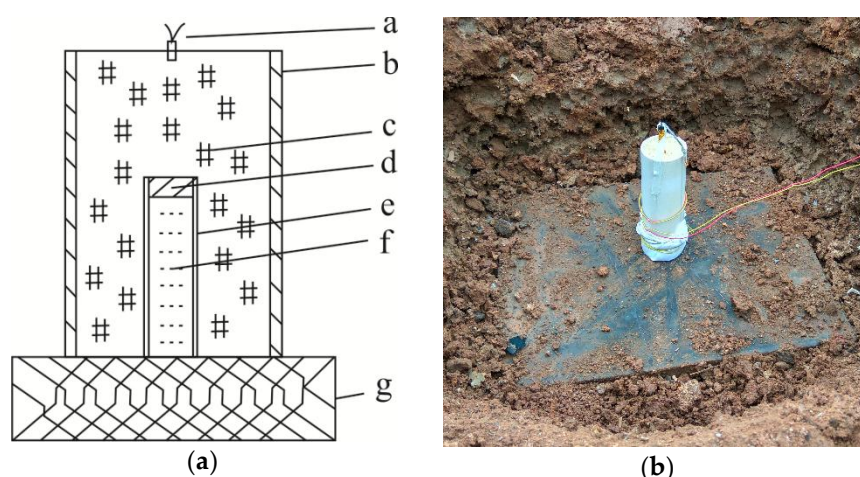
Figure 2. Schematic view (**a**) and actual diagram (**b**) of explosive consolidation device: a—detonator, b—the outer cylinder, c—emulsion explosives, d—the upper plug, e—copper tube, f—Fe-based amorphous powders, g—baseplate.

The diameter of the rod-shaped alloy formed by explosive consolidation is 8.8 mm, as shown in Figure 3. The samples of the performance test were cut through wire cutting; the two ends of the rod alloy were cut off by 10 mm to eliminate the influence of plugs, the three sections (a), (b) and (c) of rod alloy were equidistantly intercepted at the upper position, middle position and lower position of rod alloy, and the length of each section was 5 mm. The performance tests of the samples mainly included: the phase characterization of the sample was examined and analyzed by X-ray diffractometry (XRD, D/max-RB, Rigaku, Japan) with Cu-Kα radiation. The scan rate was 4$°$ min^{-1} and the scan angle range was 20–80$°$. Thermal behaviors of the samples, such as metastable phase transition temperature and transformation characteristics, were evaluated by differential scanning calorimetry (DSC, DSC 404 F3, Netzsch, Germany) at a heating rate of 10 K·min^{-1} to further determine the structure of the powder, i.e., whether it was still amorphous after explosive consolidation. The samples were put inside cylindrical yttria cups in the furnace chamber. The furnace chamber was filled with argon after vacuum-pumping. The cross-section of sample was polished, and the polishing surface was corroded with 3% nitrate alcohol. Optical micrographs of 100×, 200× and 500× magnifications were performed to determine the compaction of powders. Consequently, the morphology and surface microstructure of the sample were observed as well as analyzed with a scanning electron microscope (SEM, Hitachi S-4800, Tokyo, Japan). The density of the original powder and the samples by explosive consolidation were measured by the Archimedes method (DINGYI, ajmdsyq, Nanjing, China). The hardness of

the three sections (a), (b) and (c) of the rod alloy was measured to determine whether the explosive pressure was uniform or not throughout the sample. Before the measurement, the surfaces of the three sections (a), (b) and (c) of the rod alloy were required to be subjected to surface treatments, such as sandpaper grinding and metallographic polishing, in order to reduce the effect of work hardening on the measurement result during processing. When the hardness was measured, the radius of each section from the edge to the center of the circle up to six points were selected at the same equidistant point to measure the change in hardness in different areas of the section. Hardness was measured by depth-sensing indentation technique using a Wilson T2500 micro Vickers hardness tester (Wolpert Wilson, Norwood, MA, USA) with an applied load of 2.94 N and a holding time of 15 s; the hardness of each part was measured three times, along three different radii. The average value of the three test results was taken as the hardness of the different positions from the edge to the center of the cross-section of the sample.

Figure 3. Copper tube after explosive consolidation.

3. Results and Discussion

The XRD patterns of the original powder and explosively compacted sample are shown in Figure 4. It is notable that the XRD patterns of the original powder and the sample showed the typical amorphous diffuse peaks without sharp crystal diffraction peaks, which indicated that the rod-shaped sample still presented as amorphous after explosive consolidation. Subsequently to analysis, the main reason is that due to the transient nature of the loading of the powders and due to the concentration of the energy on the surface of the powder particles, the time that the surface temperature of the powder particles increased from room temperature to melting temperature during explosive consolidation is only microseconds. This implies that the surface of powder particles was instantaneously melted, and the generated high temperature was delayed in propagating inside the particle during explosive consolidation. This implies that the particle interior remained at a low temperature, being amorphous. The amorphous phase remained unchanged; simultaneously, the low temperature inside the powder particles could induce a cooling quenching effect on the instantly melted surfaces of the powder particles, thereby forming a dense bulk alloy. As a result, the structure of the rod-shaped alloy formed by explosive consolidation can still retain the amorphous phase consistent with powder.
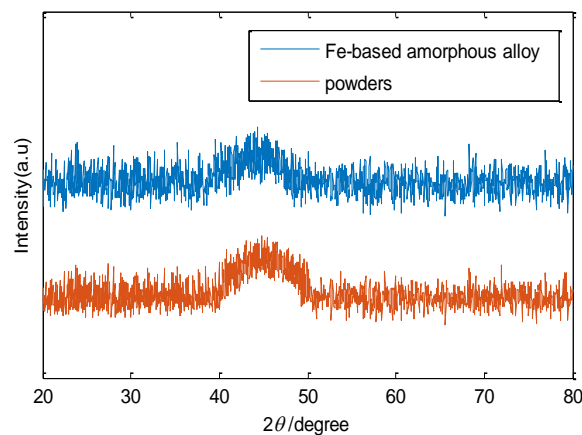
Figure 4. X-ray diffraction (XRD) patterns of the original powder and explosively compacted sample.

From the thermodynamic point of view, an amorphous alloy is in a metastable state and has high free energy [25]. Under certain conditions, it must shift towards a metastable amorphous state or an equilibrium crystalline state with lower energy. When the temperature is high, the amorphous state transitions to the equilibrium or to the metastable amorphous state lead to an exothermic process. The thermal analysis curves of the original powder and the $Fe_{61}Cr_2Nb_3Si_{12}B_{22}$ sample at a heating rate of 10 K·min^{-1} are shown in Figure 5. It could be observed that the original powder and the sample existed at the glass transition point, the liquid zone and the crystallization exothermic peak. It also appeared in multiple exothermic peaks. It demonstrated that the sample still retained the amorphous phase and had a multi-step crystallization process with the rise in temperature. The sample sustained a glass transition stage and multiple crystallization stages during the heating process. When the temperature reached 510 °C, the Fe-based amorphous alloy began to emit heat. It demonstrated that the glass transition began to occur, indicating that the glass transition temperature (Tg) of the Fe-based amorphous alloy was 784 K. The first exothermic peak appeared when the temperature was heated to 538 °C, indicating that some of the amorphous phase began to change to the crystalline phase, so the crystallization onset temperature (Tx) was 812 K, and the supercooled liquid zone (ΔTx) was 28 K; the second exothermic peak appeared at approximately 553 °C, indicating that the amorphous phase was further crystallized until the amorphous alloy was completely transformed into a crystalline material. Subsequently to two crystallization reactions, the sample transitioned from the supercooled liquid region to a stable crystallization phase; when the heating continued to 1137 °C, the alloy began to melt, so the reduced glass transition temperature (Trg) was 0.556. According to the aforementioned analysis of the sample thermal stability, it could be observed that a clear glass transition and a crystallization reaction occurred in the sample, which further proved that the structure of prepared sample is amorphous.
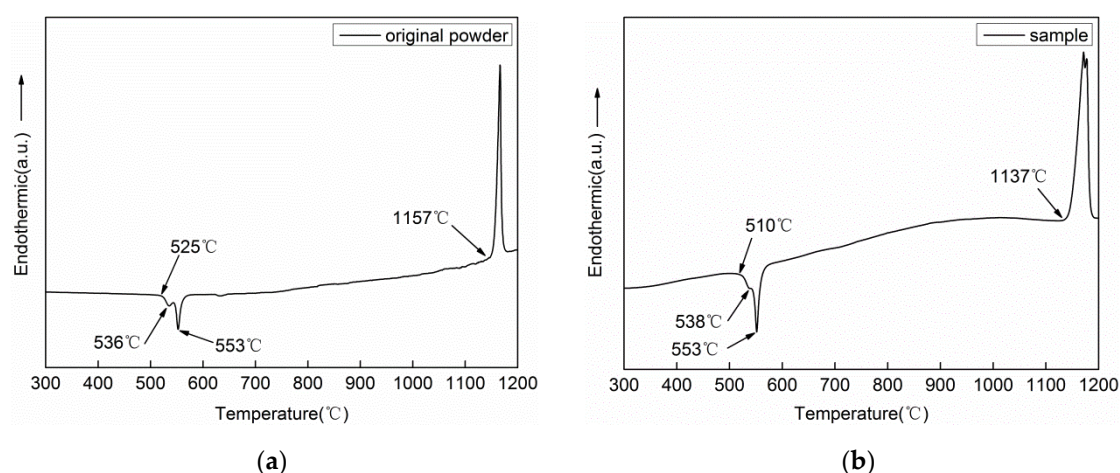
Figure 5. Differential scanning calorimetry (DSC) curves of the original powder (**a**) and the sample (**b**).

Optical micrographs of a section of the sample are shown in Figure 6. The cross-section of the sample has no macroscopic cracks. The adjacent powder particles were in contact with each other and a low amount of tiny black spots were distributed on the cross-section. This indicated that the powder particles have a high dense combination and demonstrated that the quality of the Fe-based amorphous alloy by explosive consolidation was fine.

The SEM images of the cross-section of the sample are shown in Figure 7. It was observed that the particles were tightly pressed together and the quality of the interface between them was fine. Therefore, the amorphous inter-particles were tightly bonded and achieved a high-quality sintering to form a bulk alloy during the explosive consolidation process. Also, it is important to notice that only a few cracks were generated after the explosive consolidation, which cannot be totally avoided due to the characteristics of explosive consolidation.
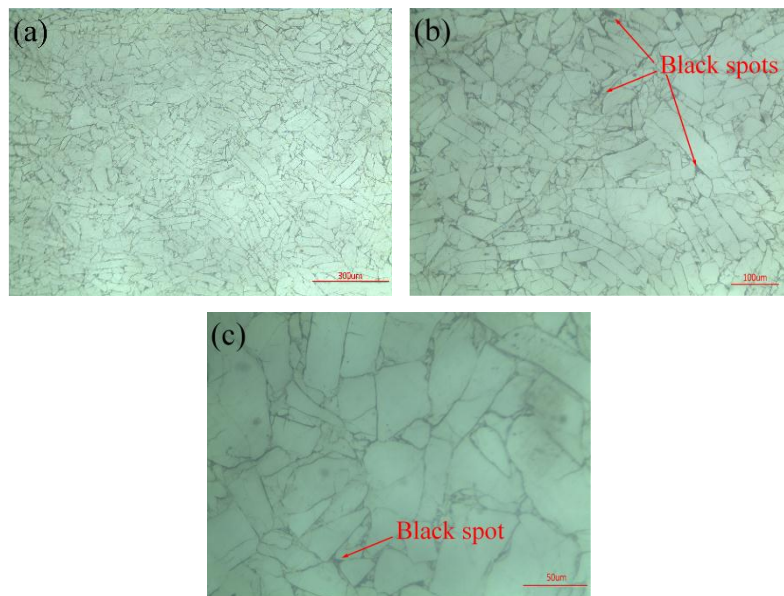
Figure 6. Optical micrographs of the cross-section of a sample: (**a**) 100× magnification, (**b**) 200× magnification, (**c**) 500× magnification.
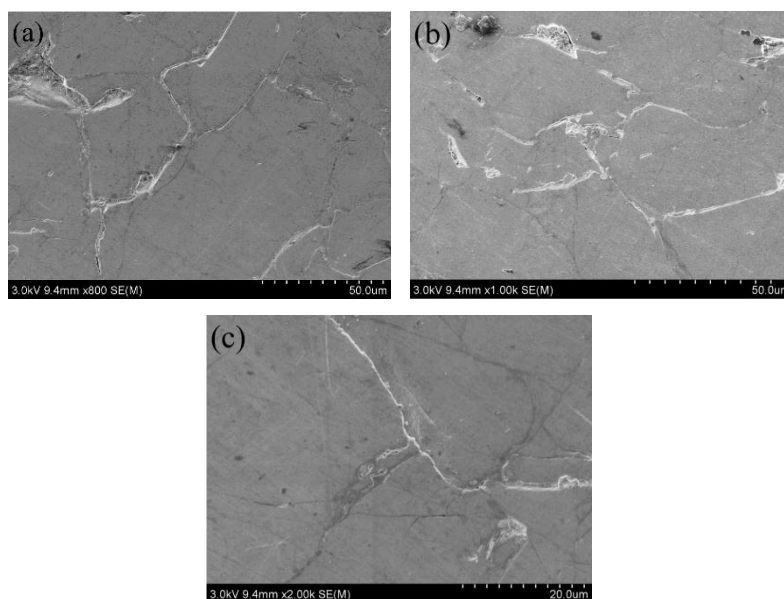
Figure 7. SEM images of the cross-section of a sample: (**a**) 800× magnification, (**b**) 1000× magnification, (**c**) 2000× magnification.

According to the optical microscopy (OM) and SEM images, it could be observed that the powder particles sustained plastic deformation, interface melting and void closure under the conditions of high temperature and high pressure at the explosion. The alloy had a high degree of dense combination.

The densities of original powder and samples by explosive consolidation are 7.18 g·cm^{-3} and 7.09 g·cm^{-3}, respectively. The density of sample reaches 98.7% of the density of the powder, indicating that the powder can reach a high-density alloy by explosive consolidation.

The micro-hardness test results of the three-section specimens are shown in Figure 8. It could be observed that the average hardness values of the three sections (a), (b) and (c) of the rod alloy were basically the same, which indicated that the detonation of the explosive had reached the stable detonation velocity when the detonation of the explosive pushed to the top of the copper tube with

powder. The minimum micro-hardness value was 1012 Hv, and the highest value was 1169 Hv, whereas the average hardness value was approximately 1069 Hv. The result demonstrated that like most Fe-based amorphous alloys, the rod alloy prepared by explosive consolidation has the excellent property of high hardness. According to the test results, the three sections had a common feature. When the micro-hardness of the specimen was near the center of the section, the hardness of the specimen changed in gradient. When the distance was 2 mm from the center, the micro-hardness of the specimen tended to be gentle and the hardness of the sample was basically unchanged. The main reason for this changed hardness of the sample was that during explosive consolidation, the surfaces of the powders were quickly heated and melted and then rapidly solidified, but the internal phase of the powders maintained at a low temperature. This is the reason that the amorphous phase structure of the sample remained unchanged and the hardness was still essentially similar to the conventional Fe-based amorphous alloys.
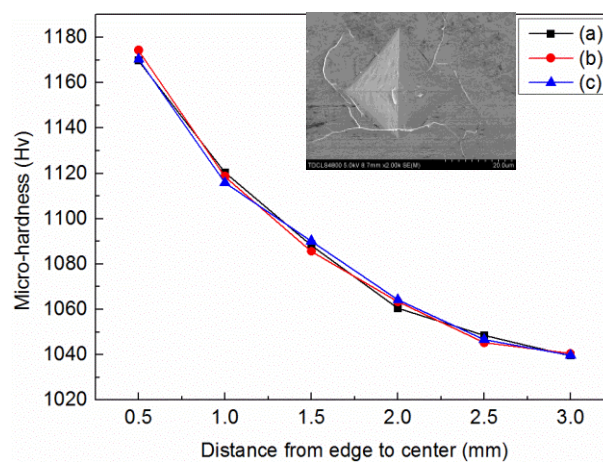
Figure 8. Change of micro-hardness from the edge to the center of the samples. Upper position (a), middle position (b) and lower position (c) of rod alloy.

The main reason for the gradient change of micro-hardness near the center of the section was that the center of the powder was a slowly melting and cooling area. In the process of explosive compaction, the powder particles in the center area had a smaller compaction distance than the powder particles in the edge area, and the power particles in the center area had less energy produced by friction between particles. The powder in the edge region was detonated first, so the powder in the center area had less energy than the powder in the edge area, and the powder in the center area was melted slowly. Also, compared with the edge area, the cooling rate of the center area was slower, which will affect the crystalline phase of the alloy to some extent, and the amorphous degree of the edge part of the alloy was better than that of the center part. This is the reason that the micro-hardness of the alloy decreased slowly from the edge to the center.

4. Conclusions

A dense bulk Fe-based amorphous alloy rod with a diameter of 8.8 mm was successfully prepared by explosive consolidation. Compared to the methods using rapid solidification, explosive consolidation can easily prepare larger size amorphous alloys and take a wider application prospect in the functional material field.

The average micro-hardness of the rod-shaped samples reached 1069 Hv, which indicated the samples had good mechanical properties. In addition, according to the micro-hardness changes from the edge to the center of the cross-section of samples, the change rules was also discovered: The micro-hardness from the edge to the center of the cross-section of samples changed gradiently and the trend of reduce change was slow.

References

1. Ghidelli, M.; Gravier, S.; Blandin, J.J.; Raskin, J.; Lani, F.; Pardoen, T. Size-dependent failure mechanisms in ZrNi thin metallic glass films. *Scr. Mater.* **2014**, *89*, 9–12. [CrossRef]

2. Han, Z.; Wu, W.F.; Li, Y.; Wei, Y.J.; Gao, H.J. An instability index of shear band for plasticity in metallic glasses. *Acta Mater.* **2009**, *57*, 1367–1372. [CrossRef]

3. Botta, W.J.; Berger, J.E.; Kiminami, C.S.; Roche, V.; Nogueira, R.P.; Bolfarini, C. Corrosion resistance of Fe-based amorphous alloys. *J. Alloy. Compd.* **2014**, *586*, 105–110. [CrossRef]

4. Janotova, I.; Hosko, J.; Svec, P.; Matko, I.; Janickovic, D.; Gemming, T.; Stoica, M. The study of structure of Fe-B-P based metallic glass. *Appl. Surf. Sci.* **2013**, *269*, 102–105. [CrossRef]

5. Gao, J.E.; Chen, Z.P.; Du, Q.; Li, H.X.; Wu, Y.; Wang, H.; Liu, X.J.; Lu, Z.P. Fe-based bulk metallic glass composites without any metalloid elements. *Acta Mater.* **2013**, *61*, 3214–3223. [CrossRef]

6. Guo, S.F.; Qiu, J.L.; Yu, P.; Xie, S.H.; Chen, W. Fe-based bulk metallic glasses: Brittle or ductile? *Appl. Phys. Lett.* **2014**, *105*, 4067. [CrossRef]

7. Yang, W.; Liu, H.; Fan, X.; Xue, L.; Dun, C.; Shen, B. Enhanced glass forming ability of Fe-based amorphous alloys with minor Cu addition. *J. Non-Cryst. Solids* **2015**, *419*, 65–68. [CrossRef]

8. Yang, W.; Liu, H.; Dun, C.; Li, J.; Zhao, Y.; Shen, B. Nearly free electron model to glass-forming ability of multi-component metallic glasses. *J. Non-Cryst. Solids* **2013**, *361*, 82–85. [CrossRef]

9. Suryanarayana, C.; Inoue, A. Iron-based bulk metallic glasses. *Int. Mater. Rev.* **2013**, *58*, 131–166. [CrossRef]

10. Hasegawa, R. Present status of amorphous soft magnetic alloys. *J. Magn. Magn. Mater.* **2000**, *215*, 240–245. [CrossRef]

11. Zheng, H.; Hu, L.; Zhao, X.; Wang, C.; Sun, Q.; Wang, T.; Hui, X.; Yue, Y.; Bian, X. Poor glass-forming ability of Fe-based alloys: Its origin in high-temperature melt dynamics. *J. Non-Cryst. Solids* **2017**, *71*, 120–127. [CrossRef]

12. Inoue, A.; Zhang, T.; Takeuchi, A. Bulk amorphous alloys with high mechanical strength and good soft magnetic properties in Fe-TM-B (TM = IV–VIII group transition metal) system. *Appl. Phys. Lett.* **1997**, *71*, 464–466. [CrossRef]

13. Lu, Z.P.; Liu, C.T.; Porter, W.D. Role of yttrium in glass formation of Fe-based bulk metallic glasses. *Appl. Phys. Lett.* **2003**, *83*, 2581–2583. [CrossRef]

14. Ponnambalam, V.; Shiflet, S.J.P.G.J.; Poon, S.J.; Shiflet, A.G.J. Fe-Mn-Cr-Mo-(Y, Ln)-C-B (Ln=Lanthanides) bulk metallic glasses as formable amorphous steel alloys. *J. Mater. Res.* **2004**, *19*, 3046–3052. [CrossRef]

15. Li, J.F.; Shao, Y.; Liu, X.; Yao, K.F. Fe-based bulk amorphous alloys with high glass formation ability and high saturation magnetization. *Sci. Bull.* **2015**, *60*, 396–399. [CrossRef]

16. Zhang, W.; Miao, H.; Li, Y.; Chang, C.; Xie, G.; Jia, X. Glass-forming ability and thermoplastic formability of ferromagnetic (Fe, Co, Ni)75P10C10B5 metallic glasses. *J Alloy. Compd.* **2017**, *707*, 57–62. [CrossRef]

17. Paul, T.; Singh, A.; Harimkar, S.P. Densification and crystallization in Fe-based bulk amorphous alloy spark plasma sintered in the supercooled liquid region. *Adv. Eng. Mater.* **2017**, *19*, 1700224. [CrossRef]

18. Li, X.J.; Wang, J.X.; Yan, H.H. The survey and development trend of the research for the mechanism of explosive consolidation of powders. *Rare Met. Mater. Eng.* **2004**, *33*, 566–570.

19. Wang, B.; Xie, F.; Wang, B.; Luo, X. Microstructure and properties of the Ti/Al$_2$O$_3$/NiCr composites fabricated by explosive compaction/cladding. *Mater. Sci. Eng. C* **2015**, *50*, 324–331. [CrossRef] [PubMed]

20. Mamalis, A.G.; Vottea, I.N.; Manolakos, D.E. On the modelling of the compaction mechanism of shock compacted powders. *J. Mater. Process. Technol.* **2001**, *108*, 165–178. [CrossRef]

21. Farinha, A.R.; Mendes, R.; Baranda, J.; Calinas, R.; Vieira, M.T. Behavior of explosive compacted/consolidated of nanometric copper powders. *J. Alloy. Compd.* **2009**, *483*, 235–238. [CrossRef]

22. Wang, J.; Zhang, X.; Zhao, Z.; Zhou, N. Explosive compaction and mechanical properties of amorphous particle reinforced Al-based amorphous composites. *Rare Met. Mater. Eng.* **2009**, *38*, 48–51.

23. Wang, B.; Xie, F.; Li, Z.; Zhang, H. Explosive compaction of Al_2O_3, nanopowders. *Ceram. Int.* **2016**, *42*, 8460–8466. [CrossRef]

24. Farinha, A.R.; Vieira, M.T.; Mendes, R. Explosive consolidation of 316L stainless steel powder—Effect of phase composition. *Adv. Powder Technol.* **2014**, *25*, 1469–1473. [CrossRef]

25. Wang, W.H.; Dong, C.; Shek, C.H. Bulk metallic glasses. *Mater. Sci. Eng.* **2004**, *44*, 45–89. [CrossRef]